

Wireless Barcodes for Tagging Infrastructure

Farnoosh Moshir

Department of Computer Science
Portland State University
Portland, OR 97207
moshir2@pdx.edu

Suresh Singh

Department of Computer Science
Portland State University
Portland, OR 97207
singh@cs.pdx.edu

ABSTRACT

There are numerous scenarios where embedding static information into objects would prove to be very useful. For example, by embedding navigation information into the road surface we could enable driverless cars, similarly embedding information into major infrastructure such as building walls would enable easier classification of debris, and so forth. The key requirement is that the embedded information should survive as long as the infrastructure itself. We discuss the concept of wireless barcodes that allow us to achieve exactly this goal of tagging infrastructure. The barcodes are designed to be read at terahertz frequencies that allows good packing of information (bits/m). We use a TDoA (Time Difference of Arrival) technique to read the barcodes which provides robustness to wear and tear of the surface. This paper reports on the results of an experimental study that examines the challenges in building such barcodes and demonstrates the idea by constructing such a barcode.

Categories and Subject Descriptors

H.4 [Information Systems Applications]: Miscellaneous;
C.2.1 [Computer Communication Networks]: Network Architecture and Design—*Wireless communication*

Keywords

Barcodes; Propagation; Terahertz

1. INTRODUCTION

Imagine a scenario where Alice is traveling in her driverless car and encounters thick fog on the isolated mountain road. Her car comes to a stop because there are no visual cues and the GPS signal is blocked by the high valley walls. In another scenario, Bob is driving along and comes to an old interesting bridge. He would like to know more about it but there are no plaques. In both these examples incorporating information into the road or the bridge would help with navigation in Alice's case and allow Bob to learn more about

Permission to make digital or hard copies of all or part of this work for personal or classroom use is granted without fee provided that copies are not made or distributed for profit or commercial advantage and that copies bear this notice and the full citation on the first page. Copyrights for components of this work owned by others than ACM must be honored. Abstracting with credit is permitted. To copy otherwise, or republish, to post on servers or to redistribute to lists, requires prior specific permission and/or a fee. Request permissions from permissions@acm.org.

MobiCom'14, September 7-11, 2014, Maui, Hawaii, USA.

Copyright 2014 ACM 978-1-4503-2783-1/14/09 ...\$15.00.

<http://dx.doi.org/10.1145/2639108.2639125>.

the bridge's history. This paper develops the concept of embedding information into infrastructure with the property that the information is as long lived as the infrastructure itself and the information can be read wirelessly. Thus, in the case of the driverless car, if we can embed *static* navigation information such as speed, steering angle, road gradient etc. into the road at periodic intervals, the car could continue driving in bad conditions. Similarly, by embedding information about the bridge into its structure, we could ensure future generations could directly read information about the bridge.

Our approach for embedding information is based on the concept of optical barcodes. However, our wireless barcodes are different in that they are read using RF and information is encoded in the accurate estimation of relative distance as opposed to intensity, as in optical barcodes. Our wireless barcodes are also entirely different from RFID tags since we use no electronic component in the wireless barcode. It is instructive to see why optical barcodes or RFID tags would be unsuitable in the two examples given previously. Optical barcodes cannot work in the presence of any form of visual impairment and they are not long lived in outdoor environments since information is stored in difference in light intensity (and possibly color). RFID tags are electronic and as such have limited life that is drastically reduced due to exposure to weather (for instance capacitors have limited life due to deterioration of the dielectric see <http://www.illinoiscapacitor.com/tech-center/life-calculators.aspx>).

1.1 Wireless Barcodes

The idea behind wireless barcodes is explained in Figure 1 where we see a signal hitting a surface which is in the shape of a step of depth d . Assuming normal incidence, the path travelled by the two reflections differ by $2d$. We can use the difference in arrival times of the two signals to embed information. If the bandwidth of the signal is large then time difference of arrival (TDoA) between the two signals will provide a reliable way of encoding information allowing us to create a barcode by using different values of d . For example, Figure 2 illustrates a barcode consisting of four *symbols* s_i each of which corresponds to a different d . In the figure we have indicated a reference surface and the information surfaces. The symbol s_i is determined based on the TDoA of the signal reflected off the *information surface* with respect to the signal reflected off the *reference surface*. If D different depths d can be reliably identified using TDoA then, in the above example, we have embedded $4 \times \log_2 D$

bits of information. Note that we need to use a reference surface because the distance between the barcode reader and the barcode can vary as a car drives or due to hand shake.

Let us return to the driverless car scenario from earlier. Imagine that we embed small plastic tags in the center of the lane of a road at some spacing. The material used can be similar to the plastic reflectors that are embedded at lane boundaries in many of the roads today. The tag contains a thin strip of reflective material (reflective to the frequency band being used) in a pattern that embeds information as in Figure 2. As the car drives along, a reader at the bottom of the car reads the embedded static information and passes it up to the navigation hardware. Thus, even in zero visibility conditions the car will be able to travel safely. In the bridge example, we could construct the barcode in the cement surface as a series of dips at a corner of the structure. A hand held reader, perhaps using a radio built into the smartphone, would be able to read the coded information.

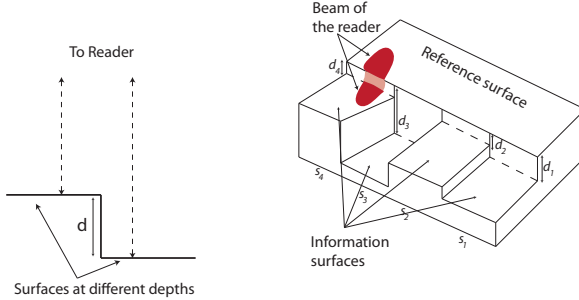


Figure 1: Encoding data using physical deformations.

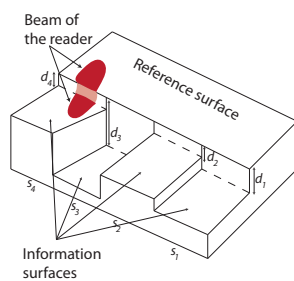


Figure 2: Example of a tag embedded in the road for navigation hints.

The size of the barcodes, specifically values of d , will affect the usability of wireless barcodes in general. For instance, it is unrealistic to use barcodes with d values in the range of several centimeters for car navigation or even labeling bridges because of the large size of the barcodes. In this paper we develop barcodes with d values measured in millimeters using terahertz radio frequencies where the large bandwidth gives us the needed precision for measuring TDoA.

1.2 Contributions and Paper Organization

In the next section we study the challenges in building barcodes based on the idea of TDoA and use Matlab simulations to illustrate the key points. Specifically, we discuss the impact of bandwidth, surface roughness and radio power on the key design parameters of barcodes. Section 3 presents the barcode design and barcode reader algorithm. Section 4 provides experimental measurements of barcode symbols built out of cement and copper. In section 4.3 we describe a prototype barcode built using copper and demonstrate the entire concept developed in this paper. We summarize optical barcodes, RFIDs, passive RF tags, chipless RF tags and terahertz tags in section 5. We conclude in section 6.

2. CHALLENGES

There are many possible designs for barcodes that use the idea of encoding data using TDoA including 2D barcodes. However, all these designs are conceptually similar and therefore we focus only on linear barcodes. We assume

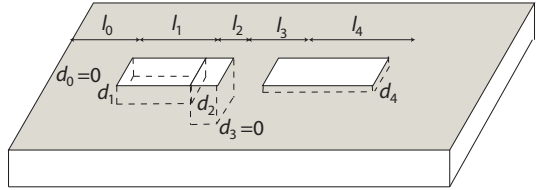


Figure 3: Example of a linear wireless barcode.

that the barcode reader emits a narrow *collimated beam*¹ and the beam is moved over the barcode to read the symbols. This is similar to pen-type optical barcode readers and *for this section we assume that the beam is very narrow*. Figure 3 illustrates a linear barcode where five symbols have been encoded: $\langle d_0, l_0 \rangle, \langle d_1, l_1 \rangle, \langle d_2, l_2 \rangle, \langle d_3, l_3 \rangle, \langle d_4, l_4 \rangle$. In this example we use the length as well as depth to encode a symbol. If a barcode reader can distinguish between D different depths $\Delta d, 2\Delta d, \dots, D\Delta d$ and between K different lengths $\Delta l, 2\Delta l, \dots, K\Delta l$ then we have a total of DK possible symbols each of which can encode $\log_2 DK$ bits.

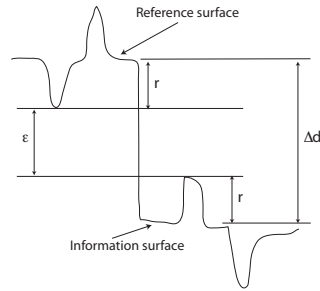


Figure 4: Relation of roughness to Δd .

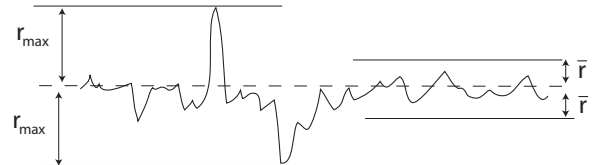


Figure 5: A 1D rough surface.

There are several factors that affect the selection of minimum depth Δd and minimum length Δl . The signal transmitted by the barcode reader may suffer from frequency-specific attenuation in the atmosphere as well as absorption and scattering in the material that forms the barcode. Indeed, the effective bandwidth used to read the barcode may well be smaller than the bandwidth of the transmitted signal. Given a reflected bandwidth of B Hz, the problem of ranging using radio echos in radar systems provides us with a lower bound on the minimum measurable Δd using TDoA techniques. If the bandwidth of the signal is B Hz then the minimal distance ϵ between two targets that can be

¹A collimated beam is one where the focus of the beam is at infinity and the diameter of the beam is the diameter of the collimating lens. Collimating beams at optical or terahertz frequencies have minimal divergence at small distances.

measured is roughly $\epsilon \propto c/2B$ meters where c is the speed of propagation [5]. For instance, if the signal reflected off the barcode has a bandwidth of 1 GHz we get $\epsilon > 15$ cm whereas, if the bandwidth is 300 GHz, then we get a more practical value $\epsilon > 0.5$ mm.

Unfortunately, we cannot expect wireless barcodes to be etched on perfectly reflective surfaces. Indeed, given the environments that motivate this research, we should expect the surfaces to be rough. Figure 4 illustrates a worst case scenario where the reference surface as well as the information surface are rough. In the figure we quantify the roughness by the maximum size of a peak or valley on the surface by r . Based on this figure, we can thus develop an estimate for Δd as the inequality: $\Delta d > \epsilon + 2r$. However, this estimate may be very pessimistic if the surface has mostly smaller bumps and valleys. A more useful model is to use the mean of r [2, 17]. For sake of explanation let us consider a one dimensional surface shown in Figure 5. Given a 90° angle of incidence of the reader signal, the time difference of arrival of various reflections off this surface will differ by up to $4r_{\max}/c$ where c is the propagation speed (this is because the maximum depth difference is $2r_{\max}$ that is doubled for round-trip time). However, an overwhelming majority of the reflected signal will arrive in a smaller time window $4\bar{r}/c$. In this case, a smaller value $\Delta d > 2\bar{r} + \epsilon$ is sufficient.

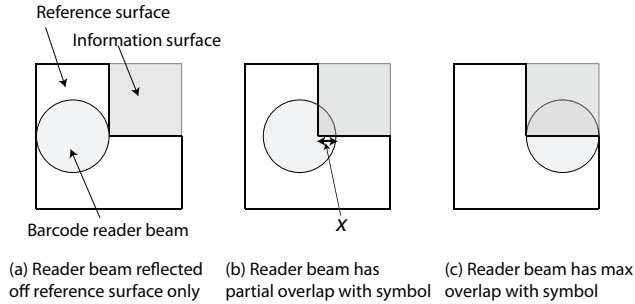


Figure 6: Detecting the start of a symbol.

The ability of the reader to detect the start and end of a symbol provides a lower bound on Δl . Consider Figure 6 where we illustrate a top view of the barcode and reader beam. The symbol is shown by the shaded box (assume it is at depth d). In Figure 6(a) the barcode reader will detect only one reflected signal of intensity P_0 . In position Figure 6(b) there are two reflected signals – one from the reference surface at intensity P_r and another from the information surface P_i . As the barcode reader beam moves to the right, P_r decreases while P_i increases as shown in Figure 6(c) when the two intensities are the same. In order to detect the start of the symbol as early as possible (to minimize error in estimating l) we need to consider three factors:

- $d > \Delta d$ to detect the symbol. Indeed if d is large then the start of the symbol can be detected earlier (for a smaller P_i) because the reflection from the information surface will be well-separated in time from the reflection from the reference surface allowing even a weak signal to be detected.
- The relative intensity $P_i/P_r > \tau(d)$ (for some threshold $\tau(d)$) in order to detect the start of the signal. As noted above, this threshold could well be dependent on d with a smaller threshold being sufficient for larger values of d .
- The total signal intensity P_0 should exceed some minimal threshold as well so that P_i/P_r is not obfuscated by noise.
- Surface roughness (denoted as σ) will diffuse the reflected signals causing two effects – a smaller value of P_i and P_r as well as spreading in time of the received signal due to variable path lengths followed by different components.

In order to examine the inter-dependence between signal intensity P_0 , bandwidth B , depth d , roughness σ and detecting the start of a symbol we conducted a simulation study in which we used two bandwidths of 10 GHz and 300 GHz. We generate a pulse and then filter it using a raised cosine filter with a roll off factor of 1 to obtain the necessary bandwidth. We consider two cases for the reflected signals – one in which the reflective surface is perfect (only noise is added) and another in which the surface is rough. We examine the perfect reflective case first to study the relationship between P_0 , B , d and Δl . Subsequently we add in a rough surface and study how this impacts the earlier analysis.

For the perfect reflective surface case, the signal received by the barcode reader $s(t)$ from a symbol at depth d can be written as,

$$\begin{aligned} s(t) &= s_r(t) + s_i(t - t_i), \text{ where } t_i = \frac{2d}{c} \\ s_r(t) &= \sqrt{\frac{P_r}{P_0}} s_0(t) \\ s_i(t - t_i) &= \sqrt{\frac{P_i}{P_0}} s_0(t - t_i) \\ |s_0(t)|^2 &= P_0 \end{aligned}$$

where P_r, P_i denotes the intensity of the signal from the reference surface and information surface respectively.

In order to identify the location of the reflections from the reference and from the information surface, we cross-correlate the received signal $s(t)$ with $s_0(t)$. Note that all barcodes indicate the start of the barcode with special symbols. In our case, we can start the barcode with just the reference surface which gives us $s_0(t)$. We compute,

$$\begin{aligned} s_0(t) \star s(t) &= s_0(t) \star \sqrt{\frac{P_r}{P_0}} s_0(t) + s_0(t) \star \sqrt{\frac{P_i}{P_0}} s_0(t - t_i) \\ &= \sqrt{\frac{P_r}{P_0}} \int_{-\infty}^{\infty} s_0(\tau) s(t + \tau) d\tau + \\ &\quad \sqrt{\frac{P_i}{P_0}} \int_{-\infty}^{\infty} s_0(\tau) s(t + \tau - t_i) d\tau \end{aligned}$$

This results in the time reversed correlation plot with two peaks corresponding to the information symbol and the reference. We apply a linear scan to the correlation data to identify these peaks (via thresholding), compute the time difference between these peaks and infer the value of d (Figures 16 and 17 show the time domain and cross-correlation plots for reading a symbol made from cement).

Relationship between $\Delta d, P_0, B$:

As a first step in our analysis, we illuminated the symbol with half the reader beam as shown in Figure 6(c). Using this setting we then determine the minimum depth Δd that can be reliably read for different values of P_0 and bandwidth. Figure 7 plots the minimum value of Δd versus P_0 . The first observation is that in all cases, the power of the reader has

a significant impact on Δd . This is to be expected since at small values of Δd the time separation of the two reflections is small and can be easily overwhelmed by noise. The second observation is that a larger bandwidth results in smaller Δd for all power values which is due to the inverse relationship between TDoA estimation and bandwidth. For a 300 GHz bandwidth, we can detect depths of as little as 0.4mm while with a 10 GHz bandwidth we can go no smaller than 8.1 mm.

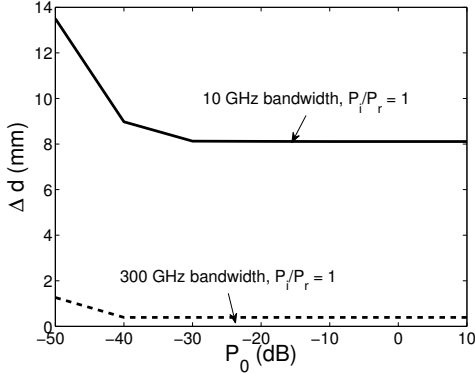


Figure 7: Min Δd versus power P_0 when $P_i/P_r = 1$.

Relationship between Δl , P_0 , P_i/P_r :

Let us use $d = 1, 2$ mm for $B = 300$ GHz and $\Delta d = 15$ mm for $B = 10$ GHz in order to determine lower bounds for Δl . Referring to Figure 6(b) we note a small overlap of the reader beam with the symbol. The value of Δl is the smallest x in the figure at which the reader can detect the symbol. As is evident, detecting the symbol is dependent on P_0 as well as the ratio P_i/P_r . This relationship is plotted in Figure 8 where we plot the *minimum* value of P_i/P_r needed to detect the symbol for different P_0 . When P_0 is small, we need almost 50% coverage of the symbol as shown in Figure 6(c) to be able to detect the symbol. Clearly in this case, the error in determining the actual start of the symbol is of the order of the beam radius. As P_0 increases past -30 dB, however, the symbols can be reliably detected when the ratio is quite small. For the 10 GHz case, the symbol can be detected when $P_i/P_r > -23$ dB while for 300 GHz, $P_i/P_r > -33$ dB is sufficient when $d = 1$ mm and $P_i/P_r > -36$ dB is sufficient when $d = 2$ mm. Note that the greater the depth d the lower the relative signal intensity needed. This makes sense since the time separation between the reference and information symbols is better allowing detection even at low power values.

If we assume a circular reader beam of radius 1 cm then we can use the minimum P_i/P_r values from above to determine the minimum value of Δl at which point we can detect the start of a symbol. This is done simply by relating the signal intensity ratio to the ratio of the area of the symbol covered by the reader beam to the area of the covered reference surface. Figure 9 plots Δl versus P_0 . As we can see for 10 GHz, $\Delta l > 0.6$ mm while for 300 GHz the values are either 0.2 mm for $d = 1$ mm or 0.1 mm for $d = 2$ mm.

Relationship of roughness σ on Δl :

Finally, we study the impact of a non-smooth surface on Δl assuming that $P_0 = 0$ dB and $B = 300$ GHz. The rough-

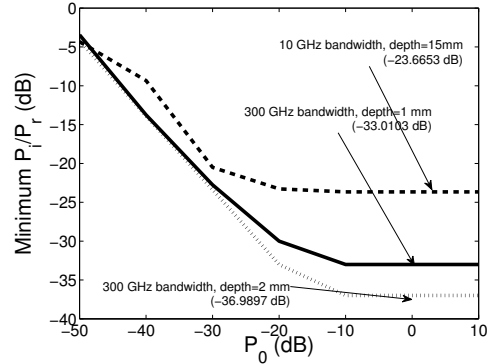


Figure 8: Minimum P_i/P_r to detect the symbol.

ness of the surface at terahertz frequencies is well modeled by a truncated zero-mean Gaussian distribution [8]. Let us assume that the random variable r from Figure 4 takes equally spaced discrete values in some range $r \in R = [-r', +r']$. For a given σ we obtain a truncated zero-mean Gaussian distribution and generate probabilities $p_r, r \in R$. We can then write $s_r(t)$ as,

$$s_r(t) = \sqrt{\frac{P_r}{P_0}} \sum_{r \in R} p_r s_0(t - t_r), \text{ where } t_r = \frac{2r}{c}$$

For our simulation shown in Figure 10 we vary $\sigma = 0$ to 0.2 for seven roughness values varying from $r = -0.3$ mm to $r = 0.3$ mm. [8] reports values of $\sigma = 0.15$ for plaster. Note that $\sigma = 0$ corresponds to the perfectly smooth case studied above. We note that Δl increases with σ as expected. Further, Δl increases faster for $d = 1$ mm. This is simply because the rough surface causes the reflected signal to spread in time and with a small d the reference signal and the information signal begin to overlap.

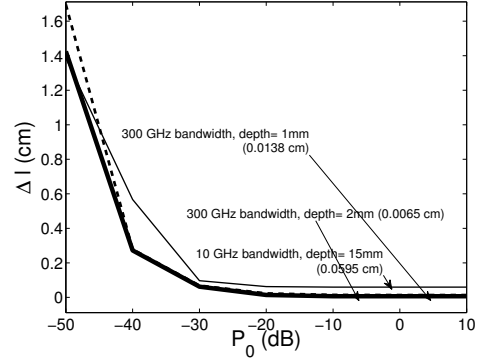


Figure 9: Minimum Δl versus power.

2.2 Summary

Our simulations clearly illustrate the relationship between B , d , Δl , σ and P_0 . For the remainder of this paper, we will focus our attention on the terahertz frequency band only due to the large available bandwidth. We will also limit ourselves to d values measured in whole millimeters because

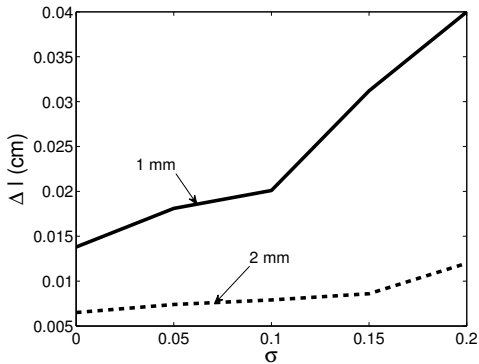


Figure 10: Minimum Δl versus variance of roughness.

surface roughness negatively affects Δl and hence it affects the length of barcode symbols.

3. BARCODE DESIGN AND READER ALGORITHM

The discussion above assumes a very narrow reader beam. While this may well be feasible in the future, the hardware we use produces a beam with a diameter of ~ 2 cm. As we see below, the diameter of the beam has a significant impact on the design of the barcode by limiting the minimum size of symbols.

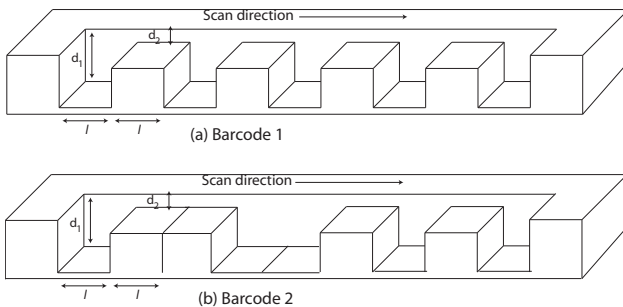


Figure 11: Example of two barcodes.



Figure 12: Reading barcodes from Figure 11 using two different beam diameters (we call it TDoA signatures).

Consider the two barcodes illustrated in Figure 11. Assume that we use the same length l for all symbols. In Barcode 1 the data encoded is: $\langle d_1, l \rangle, \langle d_2, l \rangle, \langle d_1, l \rangle, \langle d_2, l \rangle, \langle d_1, l \rangle, \langle d_2, l \rangle, \langle d_1, l \rangle$ while Barcode 2 encodes: $\langle d_1, l \rangle, \langle d_2, l \rangle, \langle d_2, l \rangle, \langle d_1, l \rangle, \langle d_1, l \rangle, \langle d_2, l \rangle, \langle d_1, l \rangle, \langle d_2, l \rangle, \langle d_1, l \rangle$. If we assume that the barcode reader has a diameter of $3l$ we obtain TDoA values as illustrated in Figure 12(a). In this plot the x-axis denotes the position of the leading edge of the reader beam. Since the reader beam is $3l$ it cannot distinguish between Barcode 1 and Barcode 2 producing exactly the same TDoA plots. If, however, we use a beam diameter of $1.5l$ we obtain the TDoA plot in Figure 12(b). The solid line in the plot corresponds to Barcode 1 while the dashed line corresponds to Barcode 2. It is easy to see that in this case we can correctly distinguish between the two barcodes. This result can be formalized as a theorem.

Theorem 1: If we assume that all the symbol lengths l are the same, then we can uniquely read a barcode if Barcode Reader Diameter $< 2l$.

Proof: Let us assume four consecutive depths (symbols) of the barcode are a, b, c, d (they do not need to be distinct). Figure 13 shows the position of the *right edge* of the reader beam over which the reader will read each of the symbols. Thus, a contributes to the TDoA measurement from the left edge of symbol a for length $l + \text{Diameter}$ (assuming Diameter $> l$). In the figure, we show the TDoA components contributed when the reader starts reading c . For segment $[3l, 2l + \text{Diameter}]$ TDoA components of a, b, c are present. For segment $[2l + \text{Diameter}, 4l]$ only components from b, c are present and from $[4l, 3l + \text{Diameter}]$ components from b, c, d are present.

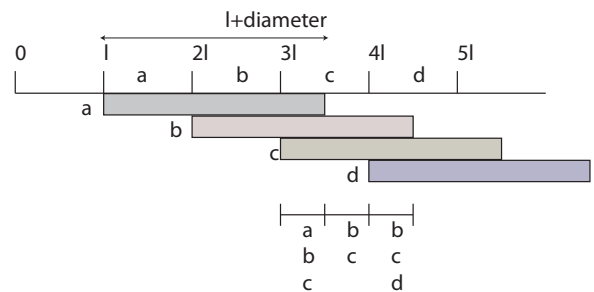


Figure 13: Illustration for Theorem 1.

Let us assume that a different barcode gives the same TDoA signature and the first symbol where these two barcodes differ is at symbol c . Let us write the TDoA signature of the two barcodes from $[3l, 3l + \text{Diameter}]$ as,

$$\begin{array}{cccc|ccc} a & b & b & a & b & b \\ b & c & c & b & e & e \\ c & d & & e & & f \end{array}$$

If we assume the two barcodes have the same signature, we need to come up with an assignment of a, b, c, d to a, b, e, f such that the two signatures are the same. Consider the different cases. If $a \neq b \neq c$ then c must equal e to make $a, b, c = a, b, e$. Similarly, if $a = b = c$ then c must again equal e to make the signatures the same. Indeed, to make $a, b, c = a, b, e$ we have no choice but to equate c and e . This means that it is impossible to construct different barcodes that yield the same TDoA signature if Diameter $< 2l$. \square

The theorem can be simply extended to the case when symbols of different length are used, but with one caveat.

Observation: The reader cannot distinguish between $\langle d, kl \rangle$ and two consecutive symbols $\langle d, ml \rangle, \langle d, (k-m)l \rangle$ for $m \geq 1$ since we do not use any kind of separator between consecutive symbols.

With the above theorem and observation in hand, we can now develop an algorithm that enables the reading of linear barcodes given a left-to-right scan direction. For ease of explanation we will assume all symbols are of the same length l . Symbols of longer lengths such as kl can be treated as k consecutive symbols of length l .

Algorithm: Assume that the barcode has been scanned and a representation of the TDoA data, as illustrated in Figure 12, is maintained. For each of the symbols d_i that appears in the barcode, we will see one or more segments as shown in the figure.

1. As a first step we delete the right hand (Diameter $- l$) portion of each segment. Thus, in Figure 12(b) if we consider the dotted line for Barcode 2, we will trim the segments $[0, 2.5l], [3l, 10.5l]$ for d_1 to $[0, 2l], [3l, 10l]$ ².
2. Since we scan left to right, at location 0 we will see a single symbol (the first symbol of the barcode). There will not be more than one symbol at position 0 since the barcode reader beam has just started overlapping the first symbol at this point. Let this symbol be d_i .
 - $Location \leftarrow 0$,
 - $Output\ symbol\ d_i$,
 - $Current\ symbols \leftarrow \{d_i\}$
3. $Location \leftarrow Location + l$
4. $Current\ symbols \leftarrow$ all symbols that are seen at this location
5. If $Current\ symbols - previous\ Output\ symbol = \{d_j\}$
 - then $Output\ symbol\ d_j$,
 - else $Output\ symbol$ is $previous\ Output\ symbol$
6. Go to 3.
7. Let nl be the total length of the barcode. There will be only one symbol whose TDoA signature extends from $[nl, (n+1)l]$. The above algorithm will output this last symbol twice. Therefore, we delete the last symbol output by the above steps and the remaining sequence of symbols denotes the complete barcode. In Figure 12(b), the TDoA signature of d_1 extends up to $10l$ (after trimming in step 1 above) since this last symbol is read by the trailing edge of the reader beam (while the leading edge is already on the right reference surface).

To see the algorithm in operation let us consider Barcode 2 in Figure 12(b). We first trim the segments for d_1 to $[0, 2l], [3l, 10l]$ and for d_2 to $[l, 4l], [5l, 9l]$. At location 0 symbol d_1 is output. Location is updated to l and $Current\ symbols = \{d_1, d_2\}$. We compute $Current\ symbols - previous$

²The notation $[a, b)$ denotes an interval that is open to the right. Therefore $b \notin [a, b)$.

$Output\ symbol = \{d_2\}$ and therefore $Output\ symbol\ d_2$. Location is incremented to $2l$. Here $Current\ symbols = \{d_2\}$ only because we have trimmed d_1 's first segment down to $[0, 2l)$. In this case $Current\ symbols - previous\ Output\ symbol$ is the null set and so $Output\ symbol\ d_2$. When location is $3l$ we have $Current\ symbols = \{d_1, d_2\}$ and thus we output d_1 . And so on. Observe that since Diameter $< 2l$ and since we trim the right Diameter $- l$ portion of each segment, we will never see 3 symbols at once.

4. PROTOTYPE COPPER AND CEMENT BAR-CODE SYMBOLS

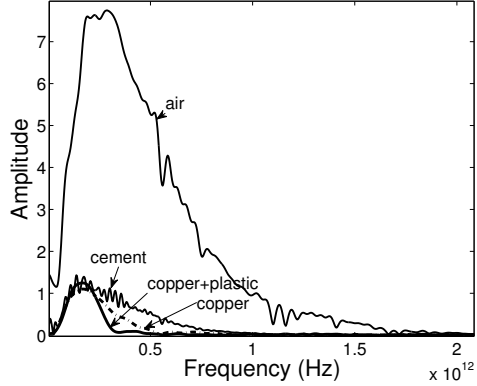


Figure 14: Spectrum of reflected signals.

Given the goal of tagging infrastructure, we construct barcode symbols from two different types of materials – copper and cement. We select copper because it provides a good reflective surface that is representative of other metallic surfaces that might be used for building such barcodes. We select cement because it is a very common building material with more roughness.

As a prelude to designing and constructing barcodes with these materials, we first measure the reflected bandwidth B of the signal. For this, we use a Picometrix 4000 Time-Domain Terahertz system that generates picosecond pulses covering up to 2 THz. In Figure 14 we plot the frequency domain of the signals reflected off cement, copper and copper covered with 0.5 cm thick plastic (this last can be used to enclose the barcode when embedded in the road). We also show the spectrum of the received pulse when traveling through free space. The dips we see in the free space plot correspond to water absorption lines (the relative humidity of the lab is set to 42%). It is interesting to note that cement has a much greater bandwidth (70-800 GHz) as compared with copper (70-500 GHz). Copper covered with thick plastic shows the smallest bandwidth (70-340 GHz). The lower end is filtered at 70 GHz to avoid interference with electronics that operate upto 70 GHz such as Wifi and 60 GHz systems.

We also conducted propagation measurements of terahertz signals as a function of distance. Figure 15 plots the received intensity as a function of distance for the case when the air is dry and when it has 42% relative humidity (RH). If we assume that the barcodes need to be read up to distances of half a meter (i.e., 1m round trip distance), the received

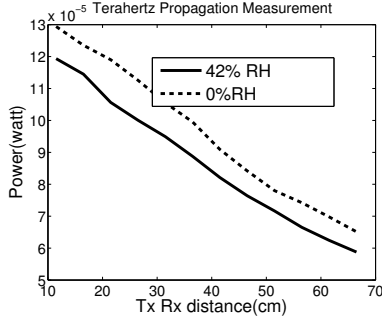


Figure 15: Measured intensity versus distance plot.

intensity will be -17.45 dBm^3 which is quite sufficient for our purposes in the car and bridge examples.

4.1 Symbol Design

The Picometrix system we use has a beam diameter of about 2cm. Therefore, given the constraint from Theorem 1, the symbols have to be at least 1cm long. The minimum symbol depth depends on the bandwidth of the signal as well as noise and other factors like roughness. Given that copper plus plastic has the smallest bandwidth of 270 GHz, we obtain a minimum $\Delta d = 0.55 \text{ mm}$. For our prototypes we decided to use $\Delta d = 1 \text{ mm}$ since it would be more robust to noise, misalignment of the barcode with respect to the reader and increased roughness.

As we noted in section 2, given D depths and K lengths there are DK possible symbols each of which can represent $\log_2 DK$ bits. We selected $D = 4$ (1 mm to 4 mm depths) because using more depths would make the barcode too bulky and thick. To select K we performed a simple optimization where the goal is to *minimize the length of the barcode*. The following theorem shows that using $K = 1$ is optimal.

Theorem 2: Given N random bits to encode, using $K = 1$ gives the minimum barcode length.

Proof: To encode N bits, we require $\lceil N/b \rceil$ symbols where $b = \log_2 DK$ bits/symbol. Since the bit stream is random, the average length of each barcode symbol will be $(K + 1)l/2$ where the lengths are $l, 2l, \dots, Kl$. Therefore the total length of the barcode is:

$$\frac{(K + 1)l}{2} \left\lceil \frac{N}{\log_2 DK} \right\rceil$$

Given that N, D, l are constant, this value is minimized at the smallest K which is 1. \square .

Therefore, for our prototype barcodes we consider $D = 4$, $l = 1 \text{ cm}$ and $K = 1$.

4.2 Individual Symbols

We constructed individual barcode symbols using quick-dry cement purchased from a hardware store. Using a simple mold (in the form of a step) we constructed symbols for the four values of d . Figure 16 plots the time-domain signal received from the symbol with $d = 1 \text{ mm}$. The two peaks we see between 0.5 and 1 correspond to the reference and the information surfaces. The first peak is the reference surface

³We use a simple linear fit to obtain this value where the received power (watts) = $-1.1279e-6 \times \text{distance} + 0.00013075$.

(closer to the reader hence the ToA is smaller). The small peaks we see around 1.5e-10 and 2.5e-10 correspond to small surface deformations in the cement. Figure 17 plots the cross-correlation of the signal with a reference signal $s_0(t)$. Note that time is reversed in the correlation plot with the y-axis being the square of the correlation coefficient. Each of the indices corresponds to 78 femtoseconds. The symbol and the reference signals are clearly visible in the plot.

We also constructed a sample barcode in copper consisting of two symbols $d = 2, 4 \text{ mm}$. Figure 18 plots the time domain signal of two symbol reflections plus the reference and Figure 19 plots the cross-correlation with a reference signal. It is trivial to identify the two symbols by using a simple linear-time thresholding algorithm. Symbol A corresponds to $d = 2 \text{ mm}$ and B corresponds to $d = 4 \text{ mm}$.

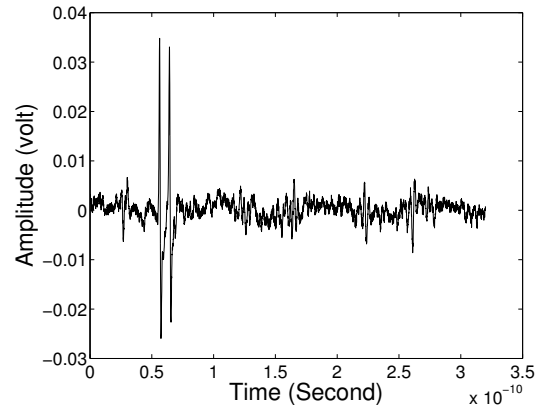


Figure 16: Reading one symbol made of cement.

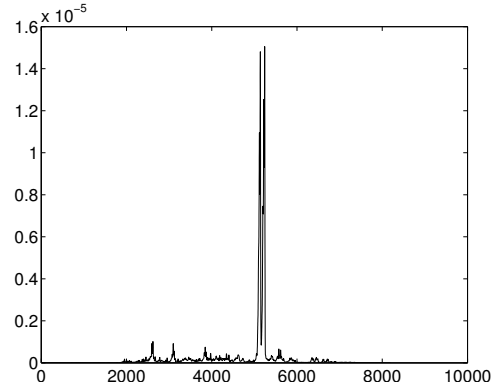


Figure 17: Cross-correlation of the time domain signals from Figure 16.

4.3 “Maui” Barcode in Copper

To demonstrate the entire concept of wireless barcodes we built a barcode in copper for the word *Maui*. We used the standard ASCII encoding for these four letters giving us 32 bits. We assigned two bits per symbol as follows: 00 – 1 mm, 01 – 2 mm, 11 – 3 mm and 10 – 4 mm. Thus, we get 16 symbols for the barcode. Since the length of each symbol was 1 cm, the total length of the barcode is 16 cm. Of course, a smaller barcode would be possible if the reader beam was narrower.

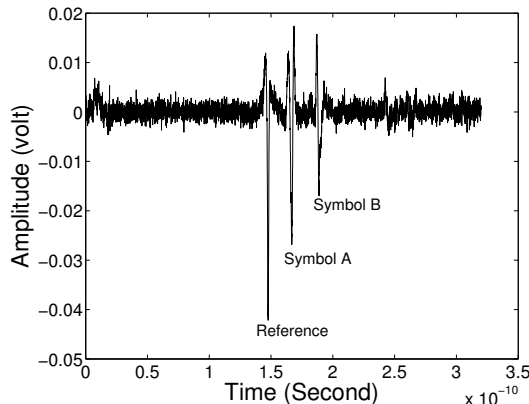


Figure 18: Reading two symbols made of copper.

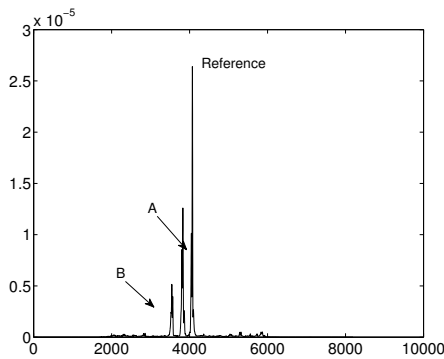


Figure 19: Cross-correlation of the time domain signals from Figure 18.

Figure 20 shows a photograph of the barcode we constructed along with the 0.5 cm thick plastic covering that we used in our measurements. This structure could potentially be embedded into a surface such as a roadway and be resistant to damage for long periods of time. The figure shows the reference surface also appears on the left and right of the barcode. this is required so we know when the barcode starts and ends. The length of the barcode in the figure is somewhat longer than 16 cm. This is because we cut and glued together the pieces to make the barcode by hand. This is also why there is a small irregularity in the reference surface around the middle point.

We read the barcode using the Picometrix system. The system moves the head in 1 mm increments. We used a single lengthwise scan of the barcode (which yields 165 individual measurements) to run our algorithm. The data produced in each scan resembles Figure 18. This is used to construct the cross-correlation plot which is then used to determine the symbols being seen. The algorithm to find the symbols is quite simple – we use a threshold to filter out all the values of the correlation plot to obtain only the maximum values of the peaks (three in the case of Figure 19). The rightmost peak is taken to be the reference surface and any peaks to the left of it are information symbols whose value is computed by using the TDoA values that can be read off from the x-axis. The 165 individual images of the barcode produced by the barcode reader when put together produce a plot like

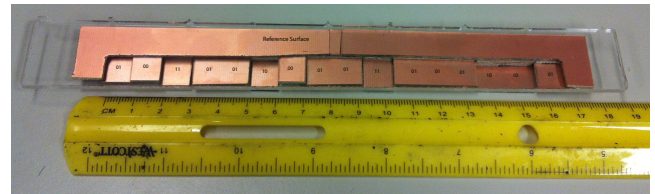


Figure 20: Photograph of the “Maui” barcode in copper.

Figure 12. We ran the algorithm described earlier on the data thus produced and the results are shown in Figure 21. Observe that symbols overlap in the plot which is because as the reader beam moves left to right it will overlap more than one symbol.

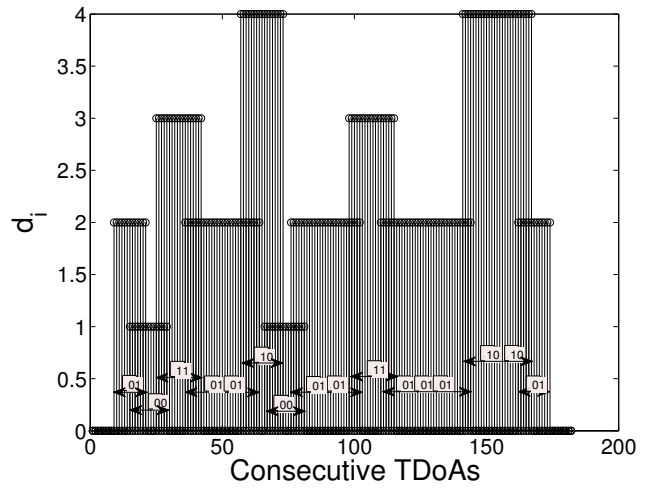


Figure 21: Reading the “Maui” barcode.



Figure 22: Barcode that was read under 1mm of water.

We also conducted an experiment to study the impact of surface roughness and water on the ability to read barcodes. For this, we built a different barcode with consecutive symbol lengths of 0.5 cm, 1cm, 1.5cm, 2cm, 2.5cm, 3cm and increasing depths from 1mm to 6mm (see Figure 22). We first scratched the surface with No. 40 sandpaper and then we stabbed it repeatedly with a screwdriver. Next we covered the barcode with 1mm layer of water. Figure 23 shows that we are able to read this barcode correctly as well. This

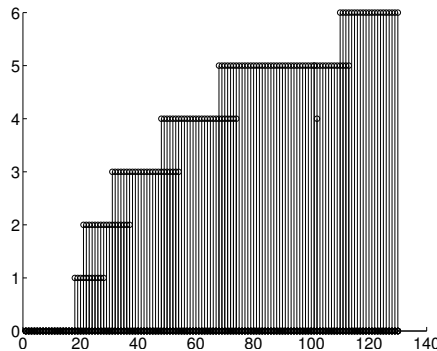


Figure 23: TDoA signature of Figure 22.

is not surprising because, as is evident from Figure 14 the bandwidth reflected by copper excludes the bands that are absorbed by water. In summary, the design we have provided appears able to meet our goals of providing a robust way to tag infrastructure.

4.4 Discussion

The results in Figures 21 and 23 were based on a single scan of the barcode. In reality, we could do multiple simultaneous scans (as is done in optical barcodes) in order to reduce reader error that will occur due to barcode degradation over time. We also note that in our design the barcodes were relatively long because the reader beam is quite wide. Given a narrow reader beam, the symbols can be made very short, of the order of 0.5mm, based on the discussion in section 2. In that case, the *Maui* barcode would shrink to less than 1cm in total length.

Readers may question the practicality of our overall barcode design concept, particularly given the fact that we used relatively sophisticated equipment for our measurements. In this context, we note that recent work on single chip design of terahertz transmitters [7],[4] and receivers [6] indicates that in the near future, handheld terahertz readers will be feasible and could also be incorporated into mobile devices. Indeed other work on small size (1 cm) high-gain antennas with 5° beams [21] for terahertz will allow incorporating highly directional terahertz beams into portable readers as well.

One of our primary motivations in this work was to enable navigation for driverless cars. Therefore an important question is whether our tags can be read at vehicular speeds v m/s. Assuming a round-trip distance of 1m between the barcode and the reader, the car will travel $\frac{v}{3}10^{-8}$ m in the time it takes the reflected pulse to return, a very small distance, even at highway speeds, given a beam radius of 0.5 mm or larger. Also note that since we use reference surfaces, the fact that the car bounces on its springs as it travels will not affect the readability of our symbols.

Finally, we note that CDs and DVDs encode single bits of information in a series of pits which appears similar to our idea, but is not. To read a CD, a beam of light is sent to the surface of the disc and depending on the presence or absence of a pit, the beam is reflected at two different angles. The receiver decodes a 1 if it receives the beam and a 0 if no beam is received. This technique can clearly not be used for tagging infrastructure because wear over time will create random reflections. Fundamentally, our technique is

different because we use TDoA to encode information while CDs use angles of reflection (and require very strict distances between the disc and the reader).

5. RELATED WORK

5.1 Optical Barcodes

The original barcodes, which are called one-dimensional barcodes, encode data by alternating the intensity of reflection along one dimension. These intervals usually are parallel black and white strips with different widths on a smooth surface. Information is encoded by varying the width of these black and white strips. Optical readers typically found in grocery stores perform multiple parallel reads of the whole barcode all at once. This allows robust error correction. Universal product code (UPC), International Article Number (EAN-13), and code 39 are some examples of the most widely used one-dimensional barcodes, [1, 11].

Two-dimensional (matrix) barcodes represent data in a two-dimensional matrix of pixels. Therefore, in comparison with one-dimensional barcodes, two-dimensional barcodes can represent more data per unit area. DataMatrix, MaxiCode, PDF417, and QR code are some examples of this barcode category. Here, image processing methods are used to extract data from patterns presented in both horizontal and vertical components of the barcode.

5.2 RFID (Radio Frequency Identification)

RFID is a technique for identifying objects with RF signals. The tag stores information electronically. A reader sends an RF signal to the tag and reads the tag's response. The reader maintains the electromagnetic field to power the tag during the half duplex transmission and reception. Because RF signals are used, the information can be read in a non-line-of-sight (NLOS) channel between reader and tag unlike optical barcodes. RFID operation frequencies are in the UHF band around 900 MHz and 2.4 GHz, and in SHF band at 5.8 GHz [19]. Recently, [13] demonstrated an entirely novel approach for battery-free communication between both the devices. The communicating devices use ambient radio signals (e.g., broadcast TV signals) for power as well as for carrying information. They have demonstrated data rates as high as 1 kbps at distance of under 2.5 feet.

5.3 Chipless RFID tags (RF Barcodes)

Encoding data in RF barcodes is different from classical RFID tags. In the RF technique, the reader transmits a RF signal to the tag. The reflected signal from the tag has a specific shape depending on the tag structure. These different electromagnetic footprints are used to encode data on RF tags. Here, there are no transmission protocols between reader and the tag. Therefore, chipless RF tags are much simpler than RFID tags.

In 2002, Hartmann [10] introduced the first chipless RF tags. These tags had antennas that receive and guide the RF signal into a Surface Acoustic Wave (SAW) substrate. Then several reflectors on the SAW substrate reflect the received signal at specific times, in what is called a time domain approach (TDA). These differences in time of the reflections are used to encode data.

In 2005, Jalaly and Robertson [12] introduced chipless RF tags without antennas. These tags have arrays of metallic strips that behave as resonant bandpass or band stop

	[10]	[16]	[12]	[19]
No. bits	2	23	5	22.9
Tag size (mm)	1	10.8×6.4	18×2.5	20×40
Info. density (bits/meter)	1,000	1,797	1,000	572

Table 1: Encoding density of chipless tags.

filters tuned to predetermined frequencies. In this technique, which is called frequency-domain approach (FDA), resonators resonant some specific frequencies. Therefore, presence or absence of resonance at a known frequency is used to encode data.

Later, in 2009, Preradovic et al. [16] used spiral resonators and were able to encode 35 bits of data. However, In the technique that Jalaly and Robertson, and Preradovic et al. have used, each bit requires one resonator. Therefore, the the size of the RF is relatively big. Mukherjee [14] and Balbin and Karmakr [3] used phase differences to encode data on the RF tag.

In 2011, Vena et al. [19] increased the RF tag data capacity by proposing a hybrid method that uses both phase and frequency to encode data. The authors have designed their RF tag with multiple metallic "C-shape" resonator elements. The structure specification of each of these resonators create a specific electromagnetic footprint when the tag is illuminated by an RF signal.

We can compare our barcodes against RFID tags in term of cost of the tag, reader cost, usability in infrastructure applications and scalability. It is easy to see that our barcodes are inexpensive though the reader cost is higher. Let us now consider scalability and use in infrastructure (we ignore the obvious frailty of RFID tags for the moment). A key limitation we note is that RFID tags cannot be placed too close to one another because these tags do not run any form of MAC protocol and thus illuminating more than one such tag will cause corrupted data at the reader. The simplest design would require tags of length l to be separated by a distance l so that the reader is only seeing one tag at once as it moves. Using the information from the first two rows of Table 1 we can obtain an information encoding density shown on the last row of the table ($0.5 \times$ number of bits/smallest dimension of tag — we multiply by 0.5 since tags of length l are separated by distance l). In the computation we used the smaller dimension to get an upper bound. In comparison, the information coding density of our wireless barcodes from Theorem 1 is $\frac{\log_2 D}{r}$ where r is the reader beam radius and D is the number of depths used. For example, if $r = 1$ mm and $D = 4$ then we have a density of 2 kbytes/meter. Of course, the equipment we use currently has a much greater radius but that will change in the future. It is interesting to observe that given a vehicular speed of v m/s, the data rate can be written as *Information density* $\times v$ bits/sec. For a car driving at 100 kmph, our 2 bit design above yields a data rate of 54 kbps.

5.4 Ultrasound Identification (USID) Tags

These tags transmit ultrasonic signals to advertise their location to readers. Unlike RFID tags, these tags are more resistant to multi-path, though they do require use of directional microphones for detection. It is interesting to consider whether ultrasonic waves could be used to read our barcodes

instead of terahertz or whether we could simply replace our barcodes with USID entirely. Using USID in outdoor environments suffers from the same longevity problem of RFID and other electronic technology. On the other hand, using ultrasonics to read our barcodes is an interesting question. Ultrasonic waves are significantly attenuated in air and the degree of attenuation depends on temperature, pressure, humidity and frequency. In order to be able to read our barcodes, we require a resolution of 1 mm which gives us a bandwidth of 170 kHz (we use the formula $c/2B$ from [5] where $c = 340$ m/s). The attenuation of ultrasound at this frequency is 15 dB/m at 20°C [20]. However, a more serious problem is that this frequency propagates well through cement [23] and is in fact used for detecting faults inside cement structures. Therefore, the reflected signal back at the reader will likely be extremely weak. If we use higher frequencies, we do not need to be concerned by the problem of transmission through cement but the attenuation factor increases to 80 dB/m for 500 kHz and 250 dB/m for 1 MHz. Another challenge in using ultrasonics to read our barcodes is car speed. Assuming a speed of 100 km/h and a round trip distance of 1 m between the reader and barcode, the car will have traveled 8 cm in the time it takes an ultrasonic pulse to return. Given that cars drive at variable speeds, the reader design and placement is challenging.

5.5 Terahertz Tags

Tedjini et al. [18] for the first time extended the concept of RF tags to the THz domain. In THz tags, data is encoded in the volume of the tag. Therefore, the security of the THz tags is greater than RF tags. In THz tags a periodic structure of two dielectric layers with different refractive indexes will exhibit ranges of forbidden frequencies when the electromagnetic signal propagates through the tag. Breaking the periodicity of the structure will create narrow defect modes in the forbidden bands. Tedjini et al. have encoded data by using the presence or absence of these defect modes at different frequency positions. The authors used high resistive silicon wafers that are separated by layers of air. Changing the thickness of the air layer in the center of the structure breaks the periodicity of the structure and causes defects in the forbidden band gap (FBG) around 150 GHz frequency. This THz tag creates four different FBGs. However, because of the thickness dispersion of the silicon wafer, the last three FBGs are damaged and only the first FBG is useable. The authors were able to encode 2 bits of data on each THz tag.

Hamdi et al. [9] also used the same idea but they create the dialectic layers from cheaper materials and they were able to encode 10 bits of data on the frequency range of the first FBG (150–600 GHz). In another work, Perret et al. [15] believe that with an FBG-width of 254 GHz and the resolution of 1 GHz, 20 effective bits can be encoded in THz tags. The forbidden bands that are created by breaking the periodicity of dielectric layers are extremely narrow and noise can degrade their performance. The thickness of dielectric layers is in the order of μm and even a small error in their depth could cause errors.

5.6 Barcodes for Digitally Fabricated Objects

Recently there has been significant interest in embedding information into objects constructed using 3D printing technology. Of particular relevance to the present paper is an approach called Infrastructs [22] that uses terahertz radios

for reading information embedded into printed objects. The key idea is to use plastics with different refractive indices (to the terahertz frequencies) arranged in layers to encode information. When such a three dimensional structure is illuminated by a perpendicular terahertz beam, portions of the beam are reflected back from each of the boundaries between different materials. *By noting the ToA of different reflections as well as if the returned pulse has a positive peak followed by negative peak (for '0') or vice versa (for '1'), the encoded information can be decoded.*

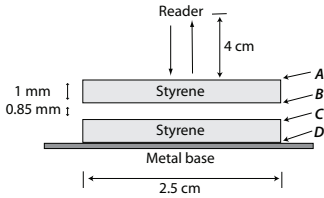


Figure 24: Infrastructure symbol.

Since Infrastructs require *transmission through layers of plastic media*, this approach is unsuitable for tagging infrastructure and severely limits what materials can be used. To illustrate this, we conducted an experiment. We constructed a simple symbol by separating two 2.5 cm square pieces of 1 mm thick Styrene sheets by an air gap of 0.85 mm and placing it on a metal plate to ensure good reflectivity. The symbol size as well as the idea of air gaps and using a metal coating are all based on the description in [22]. We use the Picometrix 4000 system to illuminate this tag and capture the reflected pulses. Figure 24 shows the symbol and as indicated the distance between the reader and the symbol is 4 cm. We expect to see 4 reflected pulses at the four surface boundaries marked by *A*, *B*, *C*, *D*. Figure 25(a) illustrates the four reflected pulses as well as secondary reflections where the pulse bounces between various boundaries before making it back to the reader. To examine how readable this simple symbol is in the presence of normal wear, we next scratch the top surface with No. 40 sandpaper. Figure 25(b) illustrates the significant attenuation in the reflected pulses and the fact that due to the roughness, each of the reflected pulses spreads in time causing *B* and *C* to overlap. If we look carefully we see that the reflections from *B*, *C* in Figure 25(a) are – peak followed by + for *B* and then + peak followed by – for *C*. In Figure 25(b) we see two consecutive pulses with – peak followed by + peak. In other words, here we cannot distinguish *C* from *B+C*. Indeed, we see no transition similar to the one in Figure 25(a) for *C* indicating that the data encoded in *C* is lost. Finally, we used a damp cloth to lightly wet the surface of the symbol. As Figure 25(c) shows, we now only get reflections from *A* and *D*. The reflection from *D* is severely attenuated (as are the reflections from *B* and *C*) due to transmission through water. The reflection from *A* is however strong.

There are two important conclusions we can derive from this experiment. First, embedding Infrastructs into infrastructure is not beneficial because these tags will quickly become unreadable. Second, this experiment illustrates why our barcodes work well even in presence of roughness and moisture. Observe that in presence of dampness, we get a strong reflected pulse in Figure 25(c). This reflection occurs between the air/water boundary on the top surface. In our

approach, since we encode symbols using different depths with respect to a reference surface, we will continue to be able to read the symbols because this reflection is always present. Indeed, this is the point also illustrated in Figures 22 and 23. In Figure 26 we show the detail of one signal received when reading Figure 22 where it is easy to pick out the two symbols at depths 1 and 2mm with respect to the reference signal despite a rough wet surface. We also note that the cement symbols we read in Figure 16 also had a rough surface but we could read them because we only rely on the reflection from the top surfaces.

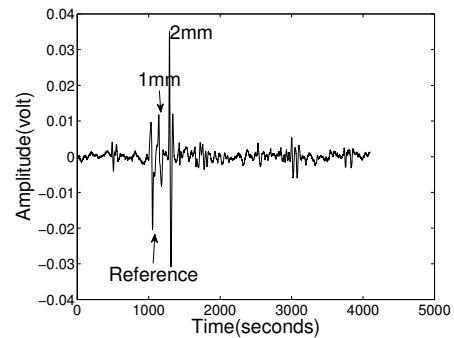


Figure 26: Detail of one signal from Figure 22.

5.7 Discussion

The barcodes we discuss in this paper are quite different from the various types of barcodes discussed above. Unlike the optical barcodes, our barcodes can be read even after significant degradation since we use TDoA rather than intensity. Unlike the chipless barcodes and the terahertz tags, our barcodes contain no electronic components or dielectric materials. Finally, unlike Infrastructs, our barcodes do not rely on transmission through material and thus can easily be built into building materials and can continue to be read despite scratches and dampness.

6. CONCLUSIONS

We present the concept of building barcodes into hard surfaces such as those used in constructing roads and bridges. The goal of these barcodes is to survive as long as the infrastructure they are built upon. In order to read the barcodes we use terahertz frequencies that enable us to have relatively small barcode symbols. We develop the underlying theory behind such barcodes and illustrate the concept using a homemade copper barcode.

Acknowledgement

This work was funded by award NSF 1217994.

7. REFERENCES

- [1] <http://en.wikipedia.org/wiki/barcode>.
- [2] R. F. Anastasi and E. I. Madaras. Terahertz nde for metallic surface roughness evaluation. In *The 4th International Workshop on Ultrasonic and Advanced Methods for Nondestructive Testing and Material Characterization*, Dartmouth, MA, 19 June 2006.

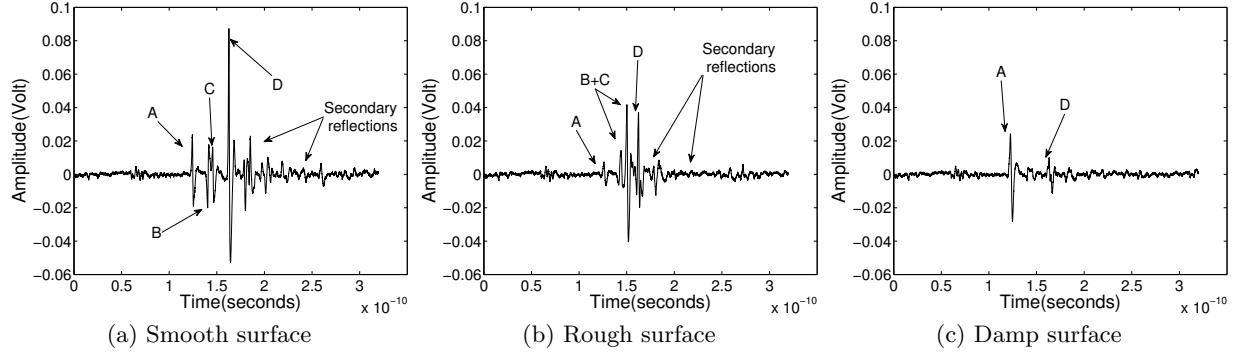


Figure 25: Measurements of a single Infrastruct symbol.

- [3] Isaac Balbin and Nemai Chandra Karmakar. Phase-encoded chipless rfid transponder for large-scale low-cost applications. *IEEE Microwave and Wireless Components Letters*, 19(8):509–511, 2009.
- [4] D. Huang et al. Terahertz cmos frequency generator using linear superposition technique. *IEEE J. Solid-State Circuits*, 43(12):2730 – 2738, 2008.
- [5] Gang Li et al. Bandwidth dependence of cw ranging to uhf rfid tags in severe multipath environments. In *IEEE International Conference on RFID*, pages 19–25, 12-14 April 2011.
- [6] H. Sherry et al. A 1kpixel cmos camera chip for 25fps real-time terahertz imaging applications. In *Proceedings IEEE ISSCC*, pages 252 – 254, 2012.
- [7] M. Feiginov et al. Resonant-tunnelling-diode oscillators operating at frequencies above 1.1 thz. *Applied Physics Letters*, 99(23), 2011.
- [8] R. Piesiewicz et al. Scattering analysis for the modeling of thz communication systems. *IEEE Transactions on Antennas and Propagation*, 55(11):3002 – 3009, November 2007.
- [9] M. Hamdi, F. Garet, L. Duvillaret, Ph Martinez, and G. Eymin-Petot-Tourtollet. New approach for chipless and low cost identification tag in the THz frequency domain. In *2012 IEEE International Conference on RFID-Technologies and Applications (RFID-TA)*, pages 24–28. IEEE, 2012.
- [10] Clinton S Hartmann. A global SAW ID tag with large data capacity. In *Ultrasonics Symposium, 2002. Proceedings. 2002 IEEE*, volume 1, pages 65–69. IEEE, 2002.
- [11] Karim Houni, Wadih Sawaya, and Yves Delignon. One-dimensional barcode reading: an information theoretic approach. *Applied optics*, 47(8):1025–1036, 2008.
- [12] I. Jalaly and I. D. Robertson. Rf barcodes using multiple frequency bands. In *2005 IEEE MTT-S International Microwave Symposium Digests*, pages 4–pp. IEEE, 2005.
- [13] V. Liu, A. Parks, V. Talla, S. Gollakota, D. Wetherall, and J. R. Smith. Ambient backscatter: wireless communication out of thin air. In *Proceedings ACM Sigcomm*, Hong Kong, August 13 – 17 2013.
- [14] S. Mukherjee. Chipless radio frequency identification by remote measurement of complex impedance. In *2007 European Conference on Wireless Technologies*, pages 249–252. IEEE, 2007.
- [15] Etienne Perret, Maher Hamdi, Guy Eymin Petot Tourtollet, Raji Nair, Frederic Garet, Anastasia Delattre, Arnaud Vena, Lionel Duvillaret, Philippe Martinez, Smail Tedjini, and Yann Boutnant. THID, the next step of chipless RFID. In *2013 IEEE International Conference on RFID (RFID)*, pages 261–268. IEEE, 2013.
- [16] Stevan Preradovic, Sushim Roy, and Nemai Karmakar. Fully printable multi-bit chipless rfid transponder on flexible laminate. In *Microwave Conference, 2009. APMC 2009. Asia Pacific*, pages 2371–2374. IEEE, 2009.
- [17] G. Sundberg, L. M. Zurk, S. Schecklman, and S. Henry. Modeling rough-surface and granular scattering at terahertz frequencies using the finite-difference time-domain method. *IEEE transactions on Geoscience and Remote Sensing*, 48(10):3709–3719, October 2010.
- [18] S. Tedjini, E. Perret, V. Deepu, M. Bernier, F. Garet, and L. Duvillaret. Chipless tags for RF and THz identification. In *2010 Proceedings of the Fourth European Conference on Antennas and Propagation (EuCAP)*, pages 1–5. IEEE, 2010.
- [19] Arnaud Vena, Etienne Perret, and Smail Tedjinil. Chipless RFID tag using hybrid coding technique. *IEEE Transactions on Microwave Theory and Techniques*, 59(12):3356–3364, 2011.
- [20] A Vladisauskas and L Jakevičius. Absorption of ultrasonic waves in air. *Ultragarsas*, 1:50, 2004.
- [21] Y. Wang, M. Ke, M. J. Lancaster, and J. Chen. Micromachined 300-ghz su-8-based slotted waveguide antenna. *IEEE Antennas and Wireless Propagation Letters*, 10:573 – 576, 2011.
- [22] Karl D. D. Willis and Andrew D. Wilson. Infrastructs: Fabricating information inside physical objects for imaging in the terahertz region. *ACM Transactions on Graphics*, 32(4):138:1 – 138:10, July 2013.
- [23] I. Q. Yaman, G. Inci, N. Yesiller, and Aktan H, M. Ultrasonic pulse velocity in concrete using direct and indirect transmission. *ACI Materials Journal*, pages 450 – 457, Nov – Dec 2001.